doi:10.14311/ppt.2025.2.99
*Plasma Physics and Technology* **12**(2):99–106, 2025 

# GLOBAL SENSITIVITY ANALYSIS OF POLYMER ABLATION MODELING FOR MAGNETOHYDRODYNAMIC FAULT ARC MODELS

F. Mingers*, S. Kimpeler, W. Leterme

*IAEW at RWTH Aachen University, Schinkelstraße 2, 52062 Aachen, Germany*

* f.mingers@iaew.rwth-aachen.de

**Abstract.** Magnetohydrodynamic fault arc model calibration presents a key challenge. The current literature lacks efficient approaches to calibrate and validate these models. A global sensitivity analysis of the ablation model is conducted to reduce the number of calibration parameters, using the Elementary Effect and Morris method. By analyzing sensitivities of calibration parameters, combined with the model outputs' standard deviation uncertainty quantification is achieved. The results help reduce uncertain parameters and improve calibration efficiency.

**Keywords:** sensitivity analysis, magnetohydrodynamics, fault arcs, switchgear, fault arc simulation.

## 1. Introduction

Complex model structures, high computational costs, and non-quantified effects, as well as interactions between modeling approaches, present challenges in magnetohydrodynamic (MHD) fault arc model calibration (see, e.g., [1]). Today, the uncertainty quantification of simulation results affected by changes in boundary conditions (BCs) plays a subordinate role in the development process of MHD fault arc models. The literature lacks efficient approaches for calibration. However, it has been shown that MHD fault arc models are capable to depict fault arc behavior and the effects on the system [2]. Nevertheless, uncertainty quantification may increase efficiency in the calibration. Global sensitivity analysis allows for the investigation of uncertain inputs and model parameters to evaluate their effects and combined effects on the predicted arc behavior (see, e.g., [3, 4]).

To enable efficient model calibration, we have tested the feasibility of the Elementary Effect Method combined with the Morris Method for polymer ablation modeling in MHD fault arc models. We characterized the sensitivity of the effective ablation enthalpy, the emissivity of the polymer surface, the Schmidt number, and the turbulent Schmidt number on the arcing energy, the pressure build-up and the polymer ablation rate using an MHD fault arc model.

This paper contributes to the quantification of data uncertainty in MHD fault arc models through global sensitivity analysis. The primary objective is to evaluate the suitability of the proposed method for extensive sensitivity analysis, including the main modeling approaches in MHD fault arc models. Furthermore, the method may support the uncertainty estimation within fault arc predictions focusing on the influence of various boundary conditions.

## 2. Uncertainty in Models

Generally, a system can be described in implicit form by a model function $f$

$$f\left(u, y, z, m, \dots\right) + \delta f(\dots) = 0. \tag{1}$$

The model includes inputs $u$, internal variables $y$, model outputs $z$, and model parameters $m$. To account for uncertainty, a model discrepancy function $\delta f(\dots)$ is defined. Different types of uncertainty, including data, model, and structural uncertainty, are incorporated into the discrepancy function and impact the prediction capability of the simulation model [5].

Data uncertainty can be either objective, based on the intrinsic randomness of a phenomenon, or subjective, based on a lack of knowledge or incomplete data [6]. Data uncertainty plays a crucial role in the calibration and validation of MHD fault arc models, as it affects both model parameters and inputs.

Model uncertainty is connected to the numerical approach itself. Usually, it occurs on a comparable small scale, as missing or incomplete physical or empirical relations are more severe than numerical errors resulting from discretization [7]. Hence, to account for model uncertainty, a discretization study was conducted prior to this study.

Structural uncertainty focuses on the overall simulation model, which is incomplete in the sense that not all possible approaches in predicting fault arc behavior can be considered. An example is the stochastic behavior of arcs, which contrasts with the deterministic nature of conventional MHD simulations. In comparison to data and model uncertainty, structural uncertainty is not directly connected to the solution quality [5]. Hence, structural uncertainty will not be considered in this study.

In the context of this study, data uncertainty refers to two main aspects. First, it arises from the lack of precise knowledge about inputs, and model parameters, which are often based on measurements or

estimates. Second, it stems from the simplified modeling approach that treats certain inputs and model parameters as constant, even though these parameters may vary over time or with environmental conditions. For the purpose of this study, we define uncertainty as a combination of (i) an input or model parameter that exhibits high relative sensitivity with respect to the outputs, and (ii) a substantial standard deviation in the output due to variability in that input or model parameter. This definition links sensitivity and output variance to identify parameters whose uncertainty has a significant impact on model predictions.

## 3. Simulation Framework

### 3.1. MHD Arc Model

Under the assumption of thermal plasma and local thermodynamic equilibrium, the Navier-Stokes equations are considered, together with the Maxwell equations in quasi-static approximation for the electric and magnetic vector potential (see, e.g., [8]). To account for the non-linearity introduced by ferromagnetic materials, the finite-element method is employed along with the finite-volume method with time-step sizes of $1 \times 10^{-15}$ s and $5 \times 10^{-7}$ s, respectively. The time-dependent equation for the magnetic vector potential is solved in the quasi-static regime, which requires the finite-element time-step size to be minimized. This approach avoids instabilities caused by large time gaps between finite-volume time steps.

The solution variables are decomposed into their mean and fluctuating components to obtain the Reynolds-Averaged Navier-Stokes equations. The realizable $k$-$\varepsilon$ model is employed in a two-layer approach. The two-layer approach is used to account for near-wall effects [9, 10].

The equations are coupled in the source term for the Lorentz force density, the temperature, pressure, and mixture dependencies of the material data, as well as the ohmic heating source density. Four source terms represent the mass and energy sources of the evaporating materials polyamide 6.6 (PA 6.6) and copper (Cu), respectively. Additionally, a momentum source term for Cu after the state transition is included [11, 12].

Thermodynamic properties, transport coefficients, and spectral data for air, PA 6.6, and Cu are provided in [13]. The transport coefficients for electrical conductivity, thermal conductivity and dynamic viscosity are calculated as a function of temperature, pressure, and gas mixture. The specific heat is calculated as a function of temperature to represent the impact of dissociation and ionization. An ideal gas is assumed; thus, gas density is calculated as a function of temperature, pressure and velocity using the ideal gas law. The convective heat transfer between gas and solids is considered at the polymer and electrode interfaces. Otherwise, a constant wall temperature of 300 K is assumed.

| Band | $\lambda_0$ / nm | $\lambda_1$ / nm |
|---|---|---|
| 1 | 33.3332 | 85.3057 |
| 2 | 85.3057 | 91.1754 |
| 3 | 91.1754 | 102.0489 |
| 4 | 102.0489 | 160.4930 |
| 5 | 160.4930 | 194.4596 |
| 6 | 194.4596 | 324.8474 |
| 7 | 324.8474 | 100 000.82 |

*Table 1. Band limits for Air-PA 6.6-Cu-mixture [14].*

Effects at the arc roots, such as anode and cathode fall voltages, are accounted for using a fractional rational function defining the current density-dependent fall voltage, as stated in [11].

The source term for radiation heat flux is calculated using the Discrete Ordinate Method (see, e.g., [15]), employing a seven-band approximation of the absorption spectrum, as outlined in table 1 [14]. The first and third band characterizes radiation processes in air [16]. At 7.725 eV and 13.6 eV, the fundamental ionization of hydrogen and copper atoms occurs, respectively [17, 18]. Therefore, band limits of 160.4930 nm and 91.1754 nm are introduced. Further ionization processes for copper are characterized by 3.82 eV and 6.38 eV. Hence, the boundaries at 324.8474 nm and 194.4596 nm are introduced, respectively [19]. The hybrid mean is used to calculate the absorption coefficients for each band [20]. The arc is initialized as a cylindrical channel of an increased electrical conductivity profile and a Gaussian distribution with the highest value of $\sigma = 5.7 \times 10^7\,\mathrm{S\,m^{-1}}$ in the center. Except the magnetic vector potential, all conservation equations are solved for finite volumes. Due to the ferromagnetic material of the vessel, the magnetic vector potential is solved for finite elements. The solution quantities are interpolated between the meshes via the method of least squares.

The model is implemented in the numerical framework of Simcenter STAR-CCM+ (2406.0001).

### 3.2. Ablation Model

Polymer vapor released during fault arcs alters the gas composition, affecting the gas properties. Neglecting processes in the Knudsen layer, the mass source $S_{\mathrm{m,PA\,6.6}}$ is calculated in each cell at the interface between the gas volume and the polymer panels, with

$$S_{\mathrm{m,PA\,6.6}} = \frac{Q_{\mathrm{w}}}{V_{\mathrm{cell}} \Delta h_{\mathrm{eff}}}. \tag{2}$$

The power $Q_{\mathrm{w}}$ accounts for the balance between radiative and convective heat flux, as well as heat conduction into the polymer. To account for the polymer's properties, the effective ablation enthalpy $\Delta h_{\mathrm{eff}}$ is introduced and multiplied by the cell volume $V_{\mathrm{cell}}$ [12]. The energy source term $S_{\mathrm{e,PA\,6.6}}$ is calculated considering the enthalpy increase of PA 6.6 during

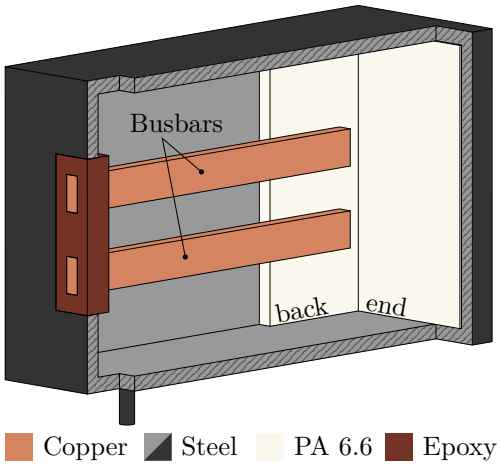


*Figure 1. Simulation model*

evaporation. The transport equation for PA 6.6 is

$$\frac{\partial}{\partial t}\int_V \rho\phi \,\mathrm{d}V + \oint_A \rho\phi\mathbf{v}\,\mathrm{d}a = \oint_A \mathbf{j}\,\mathrm{d}a + \int_V S_{\mathrm{m,PA\,6.6}}\,\mathrm{d}V, \tag{3}$$

where $\phi$ is the mass fraction of PA 6.6, $V$ is the volume, $a$ is the area vector, $\mathbf{v}$ is the velocity vector, and $\mathbf{j}$ is the diffusion flux, which is calculated as

$$\mathbf{j} = \left(\frac{\mu}{S_\mathrm{c}} + \frac{\mu_\mathrm{t}}{S_\mathrm{c,t}}\right)\nabla\phi. \tag{4}$$

$\mu$ and $\mu_\mathrm{t}$ represent the viscosity and turbulent viscosity, respectively. $S_\mathrm{c}$ and $S_\mathrm{c,t}$ are the molecular and turbulent Schmidt numbers. Additionally, equations (3) and (4) are solved for Cu mass fraction.

### 3.3. Test Setup

To limit computational costs, a geometrical reduced arrangement is implemented (Figure 1). It is based on the experimental setup published in [21]. Two horizontal busbars are placed in a hermetically sealed steel vessel (Figure 1). The vessel's inner length, width, and height are 0.31 m, 0.105 m, and 0.19 m, respectively, resulting in an inner volume of $6.18 \times 10^{-3}\,\mathrm{m}^3$. The arrangement is discretized by $2.99 \times 10^6$ finite volume and $1.36 \times 10^6$ finite element cells. The arcing current is set to a constant value of $I_\mathrm{arc} = 10\,\mathrm{kA}$ and implemented as a current density source on the outer surface of the upper busbar. The vessel and the outer surface of the lower busbar are at ground potential. The arc duration is limited to 1 ms to further limit computational costs. Due to this time restriction, we limit the investigations to the arc movement between the busbars. This circumstance must be taken into account when evaluating the results.

## 4. Methodology

To assess uncertainty, a global sensitivity analysis is conducted by defining multiple trajectories in a predefined parameter space (Section 4.2). With each set of trajectories, the convergence of sensitivity measures is calculated to define a termination criterion. Using the Elementary Effect Method, the sensitivities and interaction effects are obtained (Section 4.3). Taking the nature of each parameter, its sensitivity, and the impact of sensitivity on the model output into account, the uncertainty is evaluated.

| Parameter | Type | $\min_i$ | $\max_i$ |
|---|---|---|---|
| $S_\mathrm{c,t}$ | $m$ | 0.001 | 100.0 |
| $\varepsilon$ | $u$ | 0.01 | 0.99 |
| $S_\mathrm{c}$ | $m$ | 0.001 | 100.0 |
| $\Delta h_\mathrm{eff}$ / $\mathrm{MJ\,kg^{-1}}$ | $u$ | 5.0 | 50.0 |

*Table 2. Model parameters $m$ and inputs $u$ used and their minimum and maximum value.*

### 4.1. Investigation Parameters

The presented ablation model and its associated uncertainty, resulting from two inputs and two model parameters, are evaluated. We acknowledge the circumstances that the parameter taken into account are not exclusively responsible for uncertainty in MHD models and the ablation approach. Nevertheless, a full characterization of all inputs and model parameters would not be feasible within this study.

Equation (2) considers radiative and convective heat flux, which is calculated using the conservation equations for energy and radiation. Furthermore, $V_\mathrm{cell}$ is given through discretization. The effective ablation enthalpy $\Delta h_\mathrm{eff}$ is input to the simulation and is usually assumed to be constant or pressure-dependent, as $\Delta h_\mathrm{eff}$ decreases with pressure (see, e.g. [22]). To evaluate the influence of variable effective ablation enthalpy, $\Delta h_\mathrm{eff}$ is included in the sensitivity analysis.

Absorption of polymer surfaces is subject to wavelength and optical properties, which can be influenced either non-reversible or transient during arcing [23]. To account for absorption, the surface's emissivity $\varepsilon$ is implemented, influencing the radiative heat flux. The emissivity can be implemented either constant or dependent on absorption band, temperature, and pressure. Furthermore, various processes can impact $\varepsilon$, including degradation, surface roughness, and heating of the polymer. Thus, $\varepsilon$ is included in the sensitivity analysis.

The diffusion flux included in equation (3) is based on the material specification of $\mu$ and $\mu_\mathrm{t}$ as well as the two model parameters $S_\mathrm{c}$ and $S_\mathrm{c,t}$. In the literature, both are set to 1, as they are usually close to unity [24]. As the correct estimation is not sufficiently possible for fault arc events, both parameters are included in the sensitivity analysis.

In this study, the outputs of interest are limited to arcing energy $[E_\mathrm{arc}] = \mathrm{kJ}$, pressure build-up $[\Delta p] = \mathrm{kPa}$, and ablation rate of the polymer panels $[m_\mathrm{rate}] = \mu\mathrm{g\,J^{-1}}$ (Fig. 1). Focusing on fault arcs, the arc energy and pressure build-up are fundamental

parameters for the later application and safety considerations. Furthermore, the ablation rate is directly related to the ablated mass and, thus, to the pressure rise. The inputs' and model parameters' space is defined in table 2. The effective ablation enthalpy $\Delta h_{\text{eff}}$ is assumed to range from 5 to 50 $\mathrm{MJ\,kg^{-1}}$, reflecting typical values for thermoplastics under high-temperature degradation [22]. The emissivity $\varepsilon$ is varied from 0.01 to 0.99 to capture the full range of surface absorption behavior. For $S_{\mathrm{c,t}}$ and $S_{\mathrm{c}}$, we selected a wide logarithmic range from 0.001 to 100. These values encompass possible variations due to local arc-induced effects, while still respecting the commonly assumed value near unity [24].

### 4.2. Sampling Strategy

The parameter space of a model with $k$ parameters can be defined as a $k$-dimensional unit cube

$$\Omega^k = \{(x_1, \ldots, x_k) \,|\, 0 \leq x_k \leq 1,\ i = 1, \ldots, k\}\,. \quad (5)$$

We utilize the Morris method for sampling the input and model parameters $x_i$, by constructing $r$ matrices $\mathbf{B}^*$ [25]. Each row in $\mathbf{B}^*$ contains the value of $k$ parameters. $\mathbf{B}^*$ is calculated as

$$\mathbf{B}^* = \left(\mathbf{J}_{k+1,1}\mathbf{J}^T + \frac{\Delta}{2}\left[\,(2\mathbf{B}' - \mathbf{J}_{k+1,k})\,\mathbf{D}^* + \mathbf{J}_{k+1,k}\right]\right)\mathbf{P}^*, \quad (6)$$

with

$$\mathbf{B}' = \frac{1}{2}\left[(2\mathbf{B} - \mathbf{J}_{k+1,k})\,\mathbf{D}^* + \mathbf{J}_{k+1,k}\right]. \quad (7)$$

The calculation utilizes a lower triangular matrix $\mathbf{B} = (k+1) \times k$, where $\mathbf{B}'$ is either equal to $\mathbf{B}$ or its negative, $-\mathbf{B}$. Furthermore, a diagonal matrix $\mathbf{D}^* = k \times k$, taking values of $+1$ or $-1$ with equal possibility. $\mathbf{J}_{k+1,k} = (k+1) \times k$ is defined, taking values of $+1$ and $\mathbf{P}^* = k \times k$ containing in each column and row only one $+1$ which is randomly distributed. Starting with a random basis vector $\mathbf{q}^*$, $\mathbf{B}^*$ is derived. Overall, $r$ matrices $\mathbf{B}^*$ are calculated to examine sensitivities in the entire parameter space.

### 4.3. Elementary Effect Method

Due to the linear dependence of the model evaluation on the number of parameters, the Elementary Effect Method is chosen [4]. Sensitivity and interaction evaluation are carried out by statistical evaluation of the elementary effects. The elementary effect of the $i^{th}$ parameter in the $j^{th}$ matrix $\mathbf{B}^*$, is defined as

$$\mathrm{EE}_i^j(\mathbf{x}^j) = \frac{z\left(\mathbf{x}^j + \mathbf{e}_i\Delta_i\right) - z(\mathbf{x}^j)}{\Delta_i}. \quad (8)$$

where $\mathbf{x}^j$ contains the values for each parameter $x_i$ with

$$x_i \in \{0, 1/(p-1), 2/(p-1), \ldots, 1\}\,. \quad (9)$$

The perturbation $\Delta_i = [0, 1]$ of a parameter is defined by the discretization levels $p$ and $\mathbf{e}_i$ as the unit vector with value one at position $i$.

To estimate the first- and higher-order sensitivities, the modified mean $\mu_i^*$, and the standard deviation $\sigma_i$ are calculated for each parameter $x_i$ and model output $z$

$$\mu_i^* = \frac{1}{r}\sum_{j=1}^{r}\left|\mathrm{EE}_i^j\right|, \quad (10)$$

$$\sigma_i = \sqrt{\frac{1}{r-1}\sum_{j=1}^{r}\left(\mathrm{EE}_i^j - \mu_i^j\right)^2}. \quad (11)$$

The modified mean $\mu_i^*$ assesses the overall first-order influence of the $i$-th parameter on the model output $z$ [26]. As one of the inputs is dimensional, a comparison between all four parameters and their sensitivities on various model outputs is not suitable with the given measures. As proposed in [27], a scaled, dimensionless, and normalized measure, based on existing measures, is taken into account

$$S_{\mu_i^*}(i,j) = \frac{\mu_{ij}^* c_i}{\sum_{l=1}^{k}\mu_{lj}^* c_l}, \quad (12)$$

where $c_i = \max_i - \min_i$. To be unit conformal, $\Delta_i$ is replaced by $\Delta_i$ in equation (8), which is the unit-sensitive variation in the interval $\Delta_i = [\min_i, \max_i]$, such that $[z] = \left[\mu_{ij}^* c_l\right]$.

A relatively high value of $\mu_i^*$ implies a significant influence on the resulting model output, whereas a relatively low value implies a minor or even negligible influence. The standard deviation $\sigma_i$ estimates whether sensitivities are first-order or include higher-order influences [25, 26]. Higher-order influences translate to interaction effects with other inputs and model parameters. $\sigma_i$ close to zero implies first-order sensitivity without interaction effects. In contrast, high values of $\sigma_i$ imply higher-order sensitivity and, hence, interaction effects with other parameters. The scale ratio $\sigma_i/\mu_i^*$ is used to decide if $\sigma_i$ is close to zero. By introducing $S_{\mu_i^*}$, the sensitivities can be compared and put into perspective to the variability of the simulation results. Therefore, the standard deviation of the outputs across all simulations $\sigma_{\text{out}}$ is introduced.

If the target quantity is a time-dependent value, a dynamic sensitivity analysis is carried out. Whereby the definition of the elementary effects is adjusted that for $t \in \{t_1, \ldots, t_n\}$ let $z\,(t, \mathbf{x})$ be the result of the model $f$ at time $t$ with input and model parameters $x_i$. The sequential elementary effect $\mathrm{EE}_i^j(\mathbf{x}^j, t)$ are added to the sensitivity measures in equations (10), (11) and (12).

## 5. Results

The result section is divided into three parts. First, the sensitivity measures are checked for convergence (Section 5.1), as sufficient convergence is necessary to analyze the resulting sensitivities and uncertainties

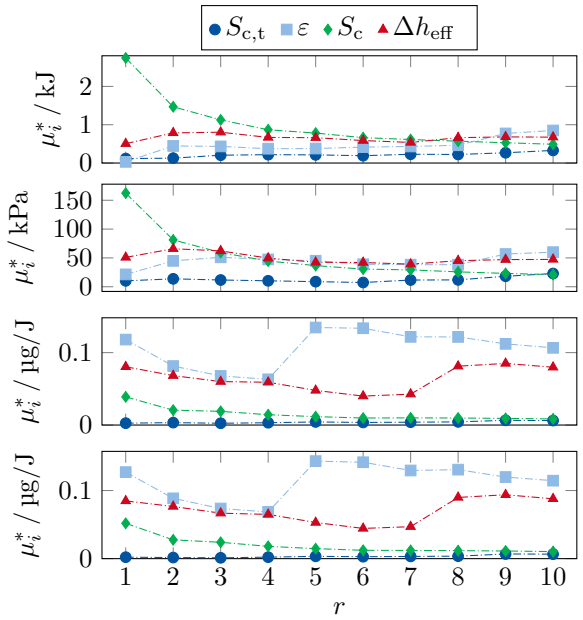


*Figure 2. Sensitivity measures $\mu_i^*$ as a function of trajectory number $r$. The four graphs include the sensitivity measures for $E_{arc}$, $\Delta p$, $m_{rate,back}$, and $m_{rate,end}$ (from top to bottom).*

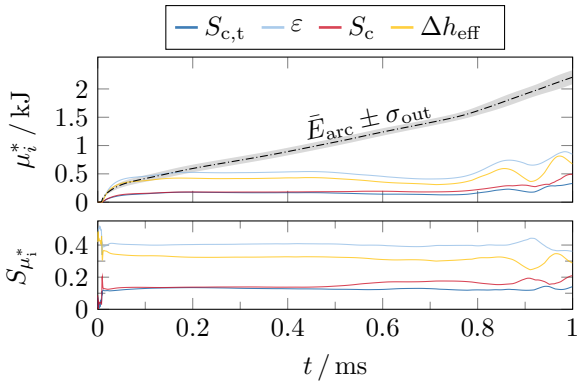


*Figure 3. Evolution of the first-order sensitivity measure $\mu_i^*$ over time. The black dash-dotted line represents the mean arc energy, and the shaded area denotes the corresponding standard deviation across all simulations. The lower graph shows the evolution of $S_{\mu_i^*}$ over time.*

reliably. Second, the global first-order sensitivity of each input and model parameter is evaluated using $\mu_i^*$ and $S_{\mu_i^*}$ (Section 5.2). In section 5.2.3, the focus is on the ablation rates for the end panel. The difference in sensitivity for all parameters between the end and back panel is negligible and, thus, will be excluded from the discussion. Third, higher-order sensitivity will be assessed by evaluating $\sigma_i$ (Section 5.3).

## 5.1. Convergence of Sensitivity Measures

In total, 50 individual simulations are performed, whereby each trajectory $r$ consists of five simulations. Each simulation consumed approximately 4600 CPU-h of computational time. Sufficient convergence of the sensitivity measures $\mu_i^*$ is achieved at a comparable low number of iterations. For all output parameters, a minimum of $r = 8$ is needed to reach sufficient convergence (Fig. 2). The mean deviation of the last three sensitivity measures compared to the sensitivity measure at $r = 10$ are 13.01 %, 12.45 %, 2.03 %, and 4.65 % for the four output parameters $E_{arc}$, $\Delta p$, $m_{rate,back}$, and $m_{rate,end}$, respectively.

## 5.2. Evaluation of Sensitivities and Uncertainty

### 5.2.1. Arcing Energy

The uncertainty of investigated parameters on the arcing energy is negligible during the acceleration along the busbars, as the sensitivity of all four parameters have a nominal influence on the standard deviation of $\bar{E}_{arc}$ (Fig. 3, upper graph). At $t = 0.8$ ms, the arc reaches the busbars' end, widens in the direction of the polymer panels, and subsequently, the influences increase. The increase in variability can be seen in $\mu_i^*$ and $\sigma_{out}$. This increase may be explained by the arc reaching the busbars' end, resulting in a higher degree of freedom for the arc movement and direct interactions with the polymer vapor in front of the PA 6.6 panels.

Generally, the ablation process itself has more influence on the arcing energy than the distribution of polymer vapor in the gas volume. The inputs are responsible for the phase shift and increase in PA 6.6 vapor, compared to the model parameters affecting only the vapor distribution. During the entire simulation time the influence of $\varepsilon$ and $\Delta h_{eff}$ are above 25 % (Fig. 3, lower graph).

Still, the influences of all four investigated parameters on the arcing energy are negligible. The standard deviation at $t = 1$ ms is 0.124 kJ at $\bar{E}_{arc} = 2.2$ kJ, which is a relative deviation of 5.67 %. Furthermore, the increase in sensitivity over time is minor, even after the arc widens. However, with increasing arcing time and decreasing distance between polymer and arc, the sensitivities become more volatile. Hence, outgassing is becoming more important as the arc duration gets longer.

### 5.2.2. Pressure Build-up

The arc's energy dissipation into the filling gas and the evaporation of solid components, adding mass to the filling gas, are responsible for the pressure build-up during fault arcs. Hence, uncertainty in pressure build-up is not only subject to the influence of the ablation model's inputs and model parameters but also propagates from the uncertainty in arcing energy. The standard deviation of the mean pressure build-up at $t = 1$ ms is 8.1 kPa at $\Delta\bar{p} = 82.47$ kPa, which is a relative deviation of 9.82 % (Fig. 4, upper graph). Similar to the mean arcing energy, the mean pressure build-up and its standard deviation increase with the arc reaching the busbars' end.

Throughout the entire simulation time, $\varepsilon$ and $\Delta h_{eff}$ have the greatest influence on the pressure build-up

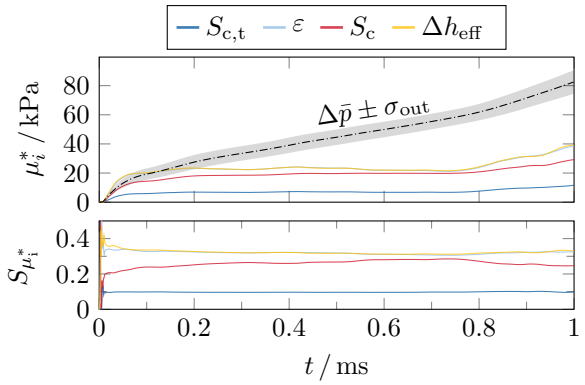


*Figure 4. Evolution of the first-order sensitivity measure $\mu_i^*$ over time. The black dash-dotted line represents the mean pressure build-up, and the shaded area denotes the corresponding standard deviation across all simulations. The lower graph shows the evolution of $S_{\mu_i^*}$ over time.*

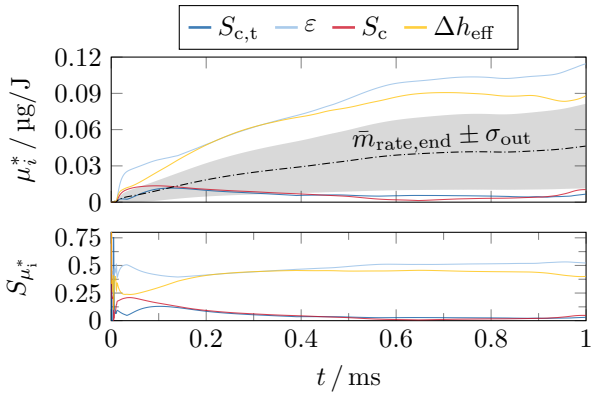


*Figure 5. Evolution of the first-order sensitivity measure $\mu_i^*$ over time. The black dash-dotted line represents the mean ablation rate, and the shaded area denotes the corresponding standard deviation across all simulations. The lower graph shows the evolution of $S_{\mu_i^*}$ over time.*

(Fig. 4, lower graph). At $t = 1\,\text{ms}$, $\varepsilon$ and $\Delta h_{\text{eff}}$ account for 39.62 % and 31.32 % of the overall influence, respectively. The comparably high sensitivity may be explained by the influence on evaporation combined with the influence on $E_{\text{arc}}$, as both affect the pressure build-up. As the arc reaches the polymer plates, the sensitivity of $\varepsilon$ and $\Delta h_{\text{eff}}$ increase, as the heat flux into the PA 6.6 panels increases by the direct arc exposure.

### 5.2.3. Ablation Rates

The uncertainty in ablation rate is the highest compared to the other model outputs. The standard deviation at $t = 1\,\text{ms}$ is $0.035\,\mu\text{g}\,\text{J}^{-1}$ at $\bar{m}_{\text{rate,end}} = 0.046\,\mu\text{g}\,\text{J}^{-1}$, which is a relative deviation of 76.09 % (Fig. 5). Since the influence on $E_{\text{arc}}$ is negligible, the influence on $m_{\text{rate,end}}$ is solely based on the ablation itself.

$\varepsilon$ and are the most sensitive parameter as their influences are at 52.20 % and 40.07 %, respectively. Whereas, the influences of $S_{c,t}$ and $S_c$ take up values of 3.02 % and 4.71 %, respectively.

It must be noted that the absolute ablation rates predicted by the model are comparable lower than those reported in experimental fault arc investigations, where values around 2 to $10\,\mu\text{g}\,\text{J}^{-1}$ are observed [28]. This discrepancy can be attributed to the short arcing time frame, which does not fully capture the long-term ablation behavior under high-energy arc conditions.

## 5.3. Interaction Effects

Generally, all sensitivities are to some extent higher-order according to the ratio $\sigma_i/\mu_i^*$ (Fig. 6). For every investigated parameter and model output, the ratio is above 1, meaning that the standard deviation of the effect is in the range and higher as the sensitivity measure $\mu_i^*$. The higher-order sensitivities may be attributed to interaction effects between parameters. Dependent on the position in the parameter space $\Omega^k$, the effect of a parameter varies and/or even changes the sign.

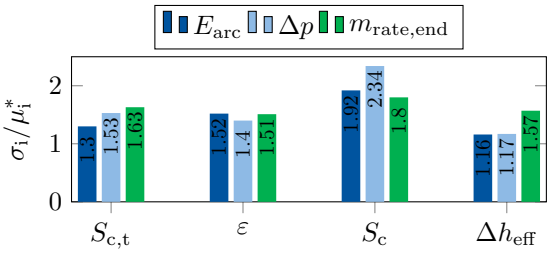


*Figure 6. The ratio of the higher-order and first-order sensitivity $\sigma_i/\mu_i^*$ at $t = 1\,\text{ms}$, as an estimate of interaction effects.*

To evaluate the origin of higher-order sensitivities, the study would need to be extended to the evaluation of two parameters at a time; however, this would exceed the scope of this study and will be part of future investigations, focusing on a limited number of parameters.

# 6. Conclusion

The Elementary Effect method, combined with the Morris method, improves the efficiency of the calibration process for MHD fault arc models by enabling the evaluation of sensitivities and interaction effects with a reasonable number of simulations. Analyzing the sensitivity measures alongside the standard deviation of the model outputs is essential for assessing the unambiguity of sensitivities and their relation to uncertainties in given modeling approaches. While the sensitivity measures identify the most influential parameters, the standard deviation indicates whether their impact needs to be considered. Hence, the number of inputs and model parameters can be reduced efficiently.

However, the elementary effect method is only applicable to parameters that are defined by a continuous or discrete interval. Numerous publications indicate the influence of radiation band selection and absorp-

tion coefficient averaging on the outputs of MHD arc models (see, e.g., [29]). As neither parameter is describable by a continuous or discrete interval, the method will need to be adapted in future research.

By analyzing the given ablation model, it can be stated that the inputs $\Delta h_{\mathrm{eff}}$ and $\varepsilon$ have a greater influence than the model parameters on the evaluated model outputs. As expected, the highest influence of the parameters is on $m_{\mathrm{rate,end}}$, with $\varepsilon$ having the highest sensitivity at more than 50 %. Thus, $\Delta h_{\mathrm{eff}}$ and $\varepsilon$ have to be taken into account in further investigations on overall model sensitivity. In future studies, $S_{\mathrm{c,t}}$ and $S_{\mathrm{c}}$ will be set constant, as their influence on the evaluated outputs is negligible. It should be noted, however, that no direct guidance for MHD fault arc models can be derived from the present study, as the analyzed arcing duration is too short in comparison to real applications. A more detailed and extended study – including longer arcing duration, higher arcing current, and a broader set of inputs and model parameters – is currently in preparation.

## Acknowledgements

Simulations were performed with computing resources granted by RWTH Aachen University under project rwth1583

## References

[1] C. Rümpler and V. R. T. Narayanan. Arc Modeling Challenges. *Plasma Physics and Technology*, 2:261–270, 2015.

[2] F. Reichert and A. Petchanka. 3D CFD Arc Fault Simulation in Gas-Insulated Switchgears. *Plasma Physics and Technology*, 6(1):35–38, 2019. doi:10.14311/ppt.2019.1.35.

[3] G. Lin and G. E. Karniadakis. Sensitivity analysis and stochastic simulations of non–equilibrium plasma flow. *International Journal for Numerical Methods in Engineering*, 80(6-7):738–766, 2009. doi:10.1002/nme.2582.

[4] S. Pfau. A sensitivity analysis method for evaluating the effect of input parameter uncertainty on the results of the PALM model system. doi:10.15488/16941.

[5] P. F. Pelz, P. Groche, M. E. Pfetsch, and M. Schaeffner. *Mastering Uncertainty in Mechanical Engineering*. Springer International Publishing, Cham, 2021. ISBN 978-3-030-78353-2. doi:10.1007/978-3-030-78354-9.

[6] D. Vandepitte and D. Moens. Quantification of uncertain and variable model parameters in non-deterministic analysis. In *IUTAM Symposium on the Vibration Analysis of Structures with Uncertainties*, volume 27 of *IUTAM Bookseries*, pages 15–28. Springer Netherlands, Dordrecht, 2011. ISBN 978-94-007-0288-2. doi:10.1007/978-94-007-0289-9_2.

[7] S. I. Repin and S. A. Sauter. *Accuracy of Mathematical Models*, volume 33. EMS Press, 2020. ISBN 978-3-03719-206-1. doi:10.4171/206.

[8] A. Gleizes, J. J. Gonzalez, and P. Freton. Thermal plasma modelling. *Journal of Physics D: Applied Physics*, 38(9):R153–R183, 2005. doi:10.1088/0022-3727/38/9/R01.

[9] W. Rodi. Experience with two-layer models combining the k-epsilon model with a one-equation model near the wall. In *29th Aerospace Sciences Meeting*, Reston, Virigina, 1991. American Institute of Aeronautics and Astronautics. doi:10.2514/6.1991-216.

[10] T.-H. Shih, W. W. Liou, A. Shabbir, et al. A new k-epsilon eddy viscosity model for high reynolds number turbulent flows. *Computers & Fluids*, 24(3):227–238, 1995. doi:10.1016/0045-7930(94)00032-T.

[11] C. Rümpler. *Lichtbogensimulation für Niederspannungsschaltgeräte*. PhD thesis, Technische Universität Ilmenau, Ilmenau, 2009.

[12] F. Reichert. *Numerische Simulation strömungsmechanischer Vorgänge in SF6-Hochspannungsleistungsschaltern*. Habilitation thesis, Technische Universität Ilmenau, Ilmenau, 2015.

[13] Y. Cressault, S. Kimpeler, A. Moser, and P. Teulet. Thermophysical Properties of Air-PA66-Copper Plasmas for Low-Voltage Direct Current Switches. *Plasma Physics and Technology*, 10(1):52–55, 2023. doi:10.14311/ppt.2023.1.52.

[14] S. Kimpeler, F. Mingers, V. West, et al. Influence of Polyamide 6.6 Ablation on Direct Current Arcs - Experiment and Simulation. *Unpublished Journal Article*, 2025.

[15] M. F. Modest. *Radiative Heat Transfer*. Academic Press, New York, 2013. ISBN 0123869447.

[16] P. Kloc, V. Aubrecht, and M. Bartlova. Numerically optimized band boundaries of Planck mean absorption coefficients in air plasma. *Journal of Physics D: Applied Physics*, 50(30), 2017. doi:10.1088/1361-6463/aa7627.

[17] S. Bashkin and J. O. Stoner. *Atomic energy-level and Grotrian diagrams*, volume I. North-Holland Publ. Co, Amsterdam, 1975. ISBN 978-0-7204-0322-0.

[18] W. Grotrian. *Graphische Darstellung der Spektren von Atomen und Ionen mit ein, zwei und drei Valenzelektronen*. Springer Berlin Heidelberg, Berlin, Heidelberg, 1928. ISBN 978-3-642-88886-1. doi:10.1007/978-3-642-90741-8.

[19] J. Sugar and A. Musgrove. Energy Levels of Copper, Cu I through Cu. *Journal of Physical and Chemical Reference Data*, 19(3):527–616, 1990. doi:10.1063/1.555855.

[20] P. Kloc, V. Aubrecht, M. Bartlova, and R. Fuchs. Comparison of Mean Absorption Methods for Radiation Transfer Models in Air Plasma at Various Pressures. *Plasma Chemistry and Plasma Processing*, 43(2):429–447, 2023. doi:10.1007/s11090-022-10304-9.

[21] T. Ballweber. *Untersuchungen zur Druckentwicklung in leistungsstarken Niederspannungs-Schaltanlagen im Störlichtbogenfall*. PhD thesis, RWTH Aachen University, 2023. doi:10.18154/RWTH-2024-00217.

[22] J.-J. Gonzalez, P. Freton, F. Reichert, and A. Petchanka. PTFE Vapor Contribution to Pressure Changes in High-Voltage Circuit Breakers. *IEEE Transactions on Plasma Science*, 43(8):2703–2714, 2015. doi:10.1109/TPS.2015.2450536.

[23] N. Bityurin, B. S. Luk'yanchuk, M. H. Hong, and T. C. Chong. Models for laser ablation of polymers. *Chemical reviews*, 103(2):519–552, 2003. doi:10.1021/cr010426b.

[24] C. K. Law. *Combustion Physics*. Cambridge University Press, 2010. ISBN 9780521870528. doi:10.1017/CBO9780511754517.

[25] M. D. Morris. Factorial Sampling Plans for Preliminary Computational Experiments. *Technometrics*, 33(2):161, 1991. doi:10.2307/1269043.

[26] F. Campolongo, J. Cariboni, and A. Saltelli. An effective screening design for sensitivity analysis of large models. *Environmental Modelling & Software*, 22(10):1509–1518, 2007. doi:10.1016/j.envsoft.2006.10.004.

[27] R. J. L. Rutjens, L. R. Band, M. D. Jones, and M. R. Owen. Elementary effects for models with dimensional inputs of arbitrary type and range: Scaling and trajectory generation. *PloS one*, 18(10), 2023. doi:10.1371/journal.pone.0293344.

[28] F. Mingers, S. Kimpeler, and W. Leterme. Experimental characterization of evaporation processes of copper and polyamide 6.6 caused by fault arcs. *Physica Scripta*, 100(7):075613, 2025. doi:10.1088/1402-4896/ade2ab.

[29] F. Reichert, J.-J. Gonzalez, and P. Freton. Modelling and simulation of radiative energy transfer in high-voltage circuit breakers. *Journal of Physics D: Applied Physics*, 45(37):375201, 2012. doi:10.1088/0022-3727/45/37/375201.